Impact of magnetite nanoparticles on the syntrophic dechlorination of 1,2-dichloroethane

Patrícia Leitão [a,b,c], Federico Aulenta [a,*], Simona Rossetti [a], Henri P.A. Nouws [c], Anthony S. Danko [b]

[a] Water Research Institute (IRSA), National Research Council (CNR), Via Salaria km. 29.300, 00015 Monterotondo, RM, Italy
[b] Department of Mining Engineering, University of Porto, Rua Dr. Roberto Frias, 4200-465 Porto, Portugal
[c] REQUIMTE/LAQV, Institute of Engineering of Porto, Polytechnic Institute of Porto, Rua Dr. António Bernardino de Almeida, 431, 4200-072 Porto, Portugal

A B S T R A C T

In anaerobic environments microorganisms exchange electrons with community members and with soil and groundwater compounds. Interspecies electron transfer (IET) occurs by several mechanisms: diffusion of redox compounds or direct contact between cells. This latter mechanism may be facilitated by the presence of conductive nanoparticles (NP), possibly serving as electron conduits among microorganisms. Our study examined the effect of magnetite (Fe_3O_4) NP on the dechlorination of 1,2-dichloroethane (1,2-DCA) by a mixed-culture. The addition of NP (170 mg L^{-1} total Fe) enhanced the acetate-driven reductive dechlorination of 1,2-DCA to harmless ethene (via reductive dihaloelimination) up to 3.3-times (2.3 μeq L^{-1} d^{-1} vs. 0.7 μeq L^{-1} d^{-1}), while decreasing the lag time by 0.8 times (23 days) when compared to unamended (magnetite-free) microcosms. Dechlorination activity was correlated with the abundance of *Dehalococcoides mccartyi*, which accounted up to 50% of total bacteria as quantified by CARD-FISH analysis, pointing to a key role of this microorganism in the process. Given the widespread abundance of conductive minerals in the environment, the results of this study may provide new insights into the fate of 1,2-DCA and suggest new tools for its remediation by linking biogeochemical mechanisms.

Keywords:
Dechlorination
Magnetite
Dehalococcoides mccartyi
1,2-Dichloroethane

1. Introduction

The chlorinated aliphatic hydrocarbon (CAH) 1,2-Dichloroethane (1,2-DCA) is commonly used as a degreasing agent and as a precursor for the production of polyvinylchloride (PVC). As such, it is frequently

detected in contaminated soil and groundwater due to improper handling, storage and disposal practices (Dinglasan-Panlilio et al., 2006).

CAHs, including 1,2-DCA, may be reduced chemically or biologically under anaerobic conditions. Microorganisms may serve as catalysts to carry out this transformation via reductive hydrogenolysis or dihaloelimination into lesser or even non-chlorinated end products. Dehalorespiration is the growth-linked process whereby microorganisms use an electron donor, such as hydrogen or acetate, and the CAHs as an electron acceptor (De Wildeman and Verstraete, 2003). Several microorganisms have been shown to carry out these reactions and include those from the genus *Dehalococcoides* (Duhamel and Edwards, 2007; He et al., 2003; Maymó-Gatell et al., 1999; Maymó-Gatell et al., 1997), *Dehalobacter* (Grostern and Edwards, 2009) and *Desulfitobacterium* (De Wildeman et al., 2003; Maes et al., 2006; Marzorati et al., 2007).

A variety of techniques have been developed for the remediation of CAHs. In-situ biostimulation of these dechlorinating populations is one technology which is commonly used due to its low cost and high environmental sustainability, when compared to other technologies (Zhang et al., 2016). This is usually done via the injection of a fermentable electron donor in the subsurface contaminated environment, such as lactate.

Recent evidence has shown that magnetite and other conductive minerals, may serve as electrical conduits to facilitate electron transfer between microbial species (Cheng and Call, 2016; Lovley, 2017). A specific example is the combination of *Geobacter sulfurreducens* and *Thiobacillus denitrificans*, which coupled acetate oxidation and nitrate reduction in the presence of magnetite nanoparticles (Kato et al., 2012). In another study, electron transfer during ethanol oxidation by *G. sulfurreducens* was facilitated by activated carbon during the reduction of fumarate by *Geobacter metallireducens* or carbon dioxide by *Methanosarcina barkeri* (Liu et al., 2012; Morita et al., 2011). Similarly, the presence of magnetite nanoparticles was found to accelerate the methanogenic conversion of organic substrates, such as propionate, by facilitating direct interspecies electron transfer (DIET) processes between acetogenic bacteria and methanogenic archaea (Baek et al., 2017; Cruz Viggi et al., 2014; Jing et al., 2017; Yang et al., 2016). Recent studies (Gacitúa et al., 2014; Zhao et al., 2016) have also shown that addition of conductive particles to the anode or cathode of bioelectrochemical systems results in enhanced electron transfer and, in turn, in a stabilized process performance. Despite its promise, the possibility to exploit magnetite-driven DIET for bioremediation applications has received, so far, only little attention. More in general, limited information is available on the interactions between minerals present (or produced) in groundwater and dechlorinating communities. Some studies have suggested that iron and manganese minerals may inhibit CAH dechlorination by serving as more suitable electron acceptors (Lu et al., 2001; Zaa et al., 2010). Others demonstrated that magnetite stimulated trichloroethene reduction using acetate as an electron donor (Aulenta et al., 2013). Interestingly, in microcosms that contained magnetite both *Desulfitobacterium* spp. and *Desulforomonas* spp. were enriched but *Dehalococcoides mccartyi* was outcompeted (Aulenta et al., 2014).

Despite these promising, yet preliminary findings, it is still unknown whether similar results may be obtained with other CAHs. Along this line, the goal of this work was to explore the impact of magnetite nanoparticles on 1,2-DCA dechlorination, which is together with TCE, the most common and dangerous chlorinated solvent occurring in subsurface environments. The need for conducting specific experiments on 1,2-DCA is also justified by the fact that this contaminant is typically degraded via a dechlorination pathway (i.e., dihaloelimination) that is different from that of TCE (i.e., hydrogenolysis).

Overall, in order to accomplish these objective, in the present study microcosm experiments were carried out to examine the impact of magnetite on 1,2-DCA dechlorination rates and lag time, as well as the interactions between different microbial community groups that are involved in the process.

2. Materials and methods

2.1. Magnetite nanoparticles synthesis

Magnetite nanoparticles were synthetized as previously described (Kang et al., 1996). In brief, the procedure consisted of successively adding the following reagents and solutions with constant stirring: 0.85 mL of 12.1 M HCl, 25 mL of ultrapure deoxygenated water, 5.2 g of $FeCl_3$ and 2.0 g of $FeCl_2$. This solution was then added dropwise under vigorous stirring to a 250 mL 1.5 M NaOH solution. The magnetic nanoparticles were isolated, by applying an external magnet, and the supernatant was decanted.

Afterwards, ultrapure deoxygenated water was added to the precipitate which was followed by centrifugation (4000 rpm) and decantation. This procedure was performed in triplicate. To neutralize the anionic charges, present on the surface of the nanoparticles, 500 mL of 0.01 M HCl was added to the precipitate under stirring. Afterwards, the solution was centrifuged (4000 rpm) and peptized with water. The magnetite nanoparticles were stored at 4 °C until use.

2.2. Mixed dechlorinating culture

The dechlorinating culture used for these experiments was an electroactive culture enriched in a microbial electrochemical system (MES) with 1,2-DCA as electron acceptor, a graphite rod as the electron donor, and antraquinone-2,6-disulfonate as redox mediator (Leitão et al., 2016). The original inoculum used for these MES experiments was activated sludge taken from a treatment plant at Roma Nord, Italy. When MES experiments ended, the content of the cathode chamber (95 mL) was anaerobically transferred to 120 mL serum bottles which were then sealed with Teflon faced butyl rubber stoppers and aluminum crimp caps. This reactor was operated in a semi-continuous mode as follows: each week, the serum bottles were sparged with N_2 to remove any remaining volatile compounds. Then, a liquid aliquot was anaerobically replaced with fresh anaerobic media, 1,2-DCA (0.05 mmol) and H_2 (0.8 mmol). The hydraulic retention time was maintained at 30 days. The reactor was operated in this manner for 4.5 hydraulic retention times (135 days) before the beginning of the experiments.

2.3. Microcosm experimental set up and monitoring

Experiments were performed in 120 mL serum bottles with a total liquid volume of 90 mL. Five different experimental conditions (Treatments A–E) were setup, each in duplicate to ensure reproducibility. Components of each treatment are listed in Table 1. The mineral medium added to each microcosm contained the following components: NH_4Cl (0.5 g L^{-1}), $MgCl_2 \cdot 6H_2O$ (0.1 g L^{-1}), K_2HPO_4 (0.4 g L^{-1}), $CaCl_2 \cdot 2H_2O$ (0.05 g L^{-1}), trace metal solution (10 mL L^{-1}) (Zeikus, 1977), vitamin solution (10 mL L^{-1}) (Balch et al., 1979), and $NaHCO_3$ (15 mL L^{-1}, 10% w v^{-1}). The pH of the medium was 7.5.

After the addition of the mineral medium, the bottles were sealed with Teflon-faced butyl rubber stoppers and aluminum crimp caps.

Table 1
Experimental setup of the microcosms. Each treatment was performed in duplicate.

Microcosms component	Treatment A	Treatment B	Treatment C	Treatment D	Treatment E
Mineral media	86 mL	88 mL	84 mL	84 mL	84 mL
Culture	–	2 mL	2 mL	2 mL	2 mL
Magnetite	4 mL	–	4 mL	4 mL	4 mL
1,2-DCA	4 μL	4 μL	–	4 μL	4 μL
Acetate	10 mM	10 mM	10 mM	–	10 mM

The bottles were then flushed with N_2 and added with 10 mL of CO_2. Subsequently, all the bottles were added with 2 mL of dechlorinating culture as inoculum (with the exception for Treatment A), 4 mL of magnetite suspension (with the exception for Treatment B), 4 μL of 1,2-DCA (with the exception for Treatment C), and acetate (from a stock solution) to a final concentration of 10 mM (with the exception for Treatment D). Upon preparation, all the microcosms were incubated upside down, in the dark, at 25 °C under mild agitation.

The microcosms were operated in a semi-continuous mode. Briefly, every two weeks, corresponding to a feeding cycle, the microcosms were purged for 10 min with N_2 to remove volatile compounds and to maintain anaerobic conditions. Thereafter, a fixed volume of liquid phase was removed from each microcosm and was replaced with fresh anaerobic medium, in order to maintain an average hydraulic and biomass retention time of approximately 120 days (Table 1). At the start of each feeding cycle, 10 mL of CO_2 was added to the headspace of the bottles and 1,2-DCA was spiked at a nominal concentration (i.e., neglecting partitioning into the gas phase) of approximately 0.6 mmol L^{-1} (but for Treatment C, which did not receive the chlorinated contaminant).

On a daily basis, all the microcosms were analyzed to determine 1,2-DCA and its reductive dechlorination products, methane, acetate, and pH, as described in the following paragraph.

2.4. Analytical methods

1,2-DCA, vinyl chlorine (VC), ethene (ETH) and methane (CH_4) were monitored by gas chromatographic analysis of headspace samples (50 μL taken with a gas-tight, gas-locking syringe). A Shimadzu GC-2014 gas chromatograph equipped with a flame ionization detector (FID) and a 2.4 m × 2.1 mm 60/80 Carbopack B/1% SP-1000 column was used, for this purpose. The GC oven temperature was initially set at 60 °C, followed by a ramp of 40 °C per minute until 180 °C which was held for 1.25 min. The carrier gas was N_2 (40 mL min^{-1}) and the temperatures of the injector and the detector were 200 °C. Headspace concentrations were converted to aqueous-phase concentrations using tabulated Henry's law constants (Gossett, 1987).

The iron load in solution was measured using an Oxford X-ray fluorescence X-MET7500 Instrument. Data were analyzed with the X-MET software by linear regression of standard solutions in the range of iron concentrations expected to be present in the microcosms.

2.5. Biomolecular analysis

For CAtalysed Reporter Deposition-Fluorescence In Situ Hybridization (CARD-FISH) analysis, 500-μL samples were collected from the inoculum and from the microcosms at the end of cycles 2, 4 and 5 with a sterile syringe and immediately fixed in formaldehyde (2% v v^{-1} final concentration) for 3 h at 4 °C. Fixed samples were filtered through polycarbonate membrane filters (pore size 0.2 μm, diameter 47 mm, Millipore) by gentle vacuum (<0.2 bar) and were then stored at −20 °C until further processing. CARD-FISH assays were performed to quantify members of *Archaea* (Arc915 probe), *Bacteria* (Eub338 I, II, III probes), *Dehalococcoides mccartyi* (Dhe1259 c and Dhe1259 t probes) and *Desulfitobacterium* spp. (Dsf440 probe plus Dsf475 helper probes) as previously described (Di Battista et al., 2012).

The probes were purchased from BIOMERS (http://www.biomers.net) and were labeled at the 50-end with horseradish peroxidase (HRP). Details of the oligonucleotide probes used are available at http://www.microbial-ecology.net/probebase. After oligonucleotide probe hybridization, total cell quantification was done by counterstaining the sample with VECTASHIELD® mounting medium containing 1.5 μg mL^{-1} of 4′,6-diamidino-2-phenylindole (DAPI) (Vector Laboratories). Visualization was performed using an Olympus BX51 epifluorescence microscope (Olympus Portugal) equipped with filters sensitive to the applied fluorochromes. Quantification of fluorescent cells was done by counting random grids on filters. All images were acquired using the Olympus CellB (Olympus Portugal) software with a magnification of 1000×. Error bars were calculated as standard deviations of cell counts using at least 5 microscopic grids for each filter.

2.6. Scanning electron microscopy (SEM) and energy-dispersive X-ray spectroscopy analysis (EDS)

Magnetite nanoparticles that were added to the microcosms were analyzed by SEM/EDS. This was done by mounting 50 μL of synthetized magnetite nanoparticles solution directly on aluminum stubs which were dried at 80 °C for 24 h.

Samples from Treatments B and E were also analyzed by SEM/EDS; at the end of the experiment, a 5 mL sample was removed and centrifuged at 5000 rpm for 5 min. After removing the supernatant, the sample was fixed in 3% (w/v) glutaraldehyde in cacodylate buffer (pH 7.2) for 3 h at room temperature. The combined mixture was centrifuged (5000 rpm, 5 min) and almost all of the supernatant was removed. A small quantity (250 μL) of the remaining solution was then mounted on an aluminum stub and dried at 50 °C for 3 h. Afterwards, the samples were dehydrated by immerging the stub with the fixed sample in 50% and 100% (v v^{-1}) (2×) ethanol solutions for 10 min each at room temperature. This was then followed by a series of hexamethyldisilazane (HMDS, Ted Pella, USA) in ethanol treatments at 50, 60, 70, 80, 90 and 2 × 100% (v v^{-1}) HMDS for 10 min each at room temperature. These dehydration steps were necessary to preserve the integrity of biological structures.

Stubs were then stored in a desiccator until SEM analysis for a maximum period of 24 h in order to prevent moisture absorption/adsorption. The samples were sputter-coated for 60 s at 15 mA current with a palladium–gold thin film using the SPI Module Sputter Coater equipment.

All samples were analyzed with a SEM/EDS system (FEI Quanta 400FEG ESEM/EDAX Genesis X4M, FEI Company, USA) in high-vacuum mode at 10 or 15 kV to observe size, morphology and distribution. X-ray microanalysis was performed in specific fields for elemental characterization.

3. Results and discussion

3.1. Kinetics of 1,2-DCA dechlorination and methane production

The effect of magnetite nanoparticles on dechlorination and methane production was evaluated in all microcosms. The concentration of iron included in the treatments with magnetite was approximately 170 mg Fe L^{-1}. Fig. 1 shows the results of dechlorination and methanogenesis rates for the different treatments for the different feeding cycles.

Treatment A was set up to evaluate if any abiotic transformation of 1,2-DCA occurred, for example by adsorption to NP's or chemical reactions. The amount of 1,2-DCA remained stable from the begin to the end of each feeding cycle. These findings seem to indicate that no abiotic 1,2-DCA transformation occurred in these microcosms. Dechlorination was observed in Treatments B, D and E, although there were differences in rates and lag times prior to the onset of the process. Dechlorination was first observed during cycle 4 (day 95) for Treatment E but only during cycle 5 (day 118) for Treatments B and D. This corresponded to a 0.8-fold decrease between Treatments E and B (Fig. S1). Maximum dechlorination rates were 3.3 times higher in Treatment E when compared to Treatment B (Fig. S2) and 50 times higher than in Treatment D (data not shown). This very low dechlorination activity in Treatment D was likely sustained by the decay of organic matter that served as an electron donor.

Under all conditions, 1,2-DCA was dechlorinated primarily via dihaloelimination to ethene, with VC (deriving from the abiotic

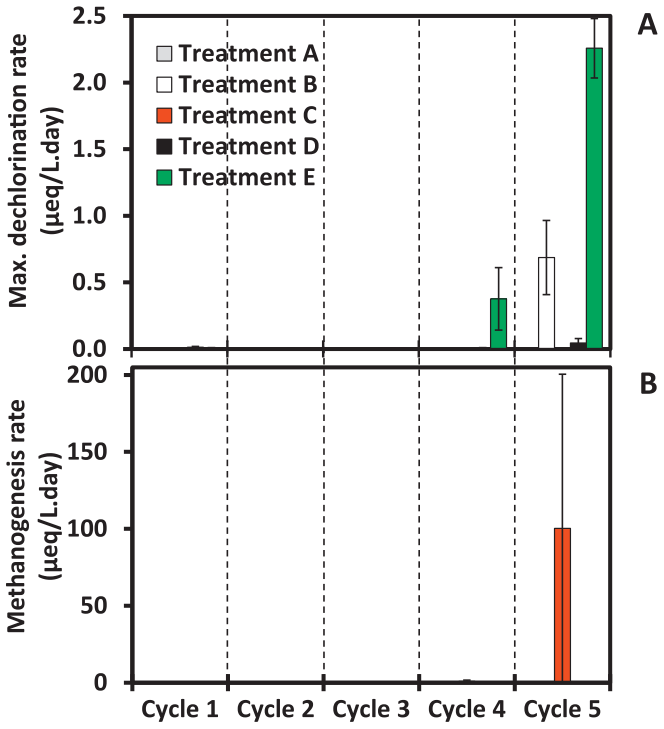

Fig. 1. Dechlorination rate (A) and methanogenesis rate (B) for the different experimental set-ups: Treatment A (not amended with the dechlorinating culture), Treatment B (not amended with magnetite), Treatment C (not amended with 1,2-DCA), Treatment D (not amended with acetate) and Treatment E (amended with all the components). Error bars represent the standard deviation of duplicates.

dehydrochlorination of 1,2-DCA) typically accounting for <1% of the removed 1,2-DCA.

Overall, the dechlorination rates obtained in this study are comparable to those reported by others. Aulenta et al., 2013 showed that the TCE dechlorination rate increased by an average of 1.5 fold in the presence of magnetite during the first two feeding cycles. Although, the iron concentration was <10 mg L^{-1}, 17 times lower than in the present study. Another study from the same group (Aulenta et al., 2014) tested the effect of filtered and untreated magnetite nanoparticles using the same inoculum. TCE dechlorinating rates increased 4.5 times (filtered magnetite particles) and 9.5 times (untreated magnetite particles) when compared to treatments without magnetite. The inoculum used in those studies was a mixture of a TCE reducing culture and an acetate-oxidizing culture (Aulenta et al., 2013). This acetate-oxidizing culture was enriched in a MES and was highly efficient and oxidized >90% of the added acetate at the anode (Villano et al., 2012), which may have contributed to the higher rates observed in that study compared to the present one. Indeed, the inoculum used in this study was not previously fed with acetate.

The highest methanogenic rate (100.30 μeq L^{-1} day^{-1}) was observed in cycle 5 for Treatment C, which did not contain 1,2-DCA. Niche adaptation of the microorganisms present might be responsible for this methanogenesis since reducing equivalents resulting from acetate oxidation could have been diverted from dechlorination towards methane production. Methanogenic rates for Treatments B and E were significantly lower than for Treatment C. The methanogenic rate observed in Treatment B was approximately 2.5 fold higher than the one obtained in Treatment E (0.0024 μeq L^{-1} day^{-1} and 0.00095 μeq L^{-1} day^{-1}, respectively).

3.2. Molecular and microscopy characterization of Archaea and Bacteria

Qualitative and quantitative analysis of *Archaea* and *Bacteria* domains using CARD-FISH of the original culture used to inoculate microcosms and of the microcosms of the treatments containing biomass at Cycles 2, 4 and 5 (Fig. 2). The abundance of archaea and bacteria in the inoculum used was $7.88 \times 10^{10} \pm 1.31 \times 10^{10}$ cell mL^{-1} and $1.66 \times 10^{11} \pm 4.17 \times 10^{10}$ cell mL^{-1}, respectively (data not shown).

Archaea abundance was consistently higher for Treatment B (2.9, 3.1 and 4.4-fold in cycles 2, 4 and 5, respectively) when compared to Treatment E.

Bacterial abundance in Treatment B initially decreased from cycle 2 to cycle 4 and increased in cycle 5 to levels similar to those found in cycle 2. The results for Treatment E showed that bacterial cell densities were lower in cycles 4 and 5 compared to cycle 2. For Treatment C, both archaea and bacteria decreased from cycle 2 to cycle 4 and then increased during cycle 5. This increase in archaea occurred at the time when methane production was observed. Interestingly, archaea cell abundance in Treatment C was lower than in Treatment B during cycle 5. This result suggests a more robust syntrophic partnership between acetate oxidizers and methanogens in the presence of magnetite without the competition from dechlorinating bacteria, which is consistent with the results of a previous study (Cruz Viggi et al., 2014). In addition, archaea cell numbers in Treatment E were lower than both Treatments B and C during this same cycle. This seems to indicate that the reducing equivalents from acetate oxidation were more efficiently transferred to the dechlorinators at the expense of methanogens. Archaeal and bacterial populations exhibit a decreasing tendency throughout the experiment in Treatment D. This was likely due to the fact that because acetate was not added, syntrophic interactions between acetate oxidizing and halorespiring microorganisms were limited.

3.3. Molecular and microscopy characterization of dechlorinating microorganisms

CARD-FISH analysis was also performed with oligonucleotide probes targeting *Desulfitobacterium* spp. and *Dehalococcoides mccartyi* in the original culture used to inoculate microcosms and in treatments containing biomass (Treatments B, C, D and E) in cycles 2, 4 and 5. The abundance of *Desulfitobacterium* spp. and *Dehalococcoides mccartyi* in the inoculum was $7.75 \times 10^{10} \pm 1.16 \times 10^{10}$ cell mL^{-1} and $2.02 \times 10^{10} \pm 7.19 \times 10^{9}$ cell mL^{-1}, respectively.

Cell densities of these two genera and maximum dechlorination rates during cycles 2, 4 and 5 for Treatments B and E are shown in Figs. 3 and 4, respectively, while the cell densities for Treatments C and D are shown in Table S1.

For Treatment B. in cycle 2, the cell density of *Desulfitobacterium* spp. was $6.8 \pm 4.6 \times 10^{9}$ cells mL^{-1} and represented 12% of total bacteria, while *Dehalococcoides mccartyi* was not detected. The cell density of *Desulfitobacterium* spp. increased to $1.78 \pm 0.18 \times 10^{10}$ cells mL^{-1} in cycle 4 and remained approximately the same in cycle 5 ($1.70 \pm 0.58 \times 10^{10}$ cells mL^{-1}). *Dehalococcoides mccartyi* was only detected in cycle 5 with a cell abundance of $1.10 \pm 0.31 \times 10^{10}$ cells mL^{-1} and the dechlorination rate was 0.69 μeq L^{-1} day^{-1}.

Micrographs of *Dehalococcoides mccartyi* and *Desulfitobacterium* spp. counterstained with DAPI in cycle 5 for Treatment B are represented in Fig. S3. The relative abundances of *Dehalococcoides mccartyi* and *Desulfitobacterium* spp. in this cycle were 28.1% and 42.1% of the total bacteria, respectively.

Cell abundance of *Dehalococcoides mccartyi* and *Desulfitobacterium* spp. and maximum dechlorination rates for Treatment E are shown in Fig. 4. The results obtained for cycle 2 are similar to those for Treatment B, where *Dehalococcoides mccartyi* was not detected while cell abundance of *Desulfitobacterium* spp. was $1.11 \pm 0.24 \times 10^{10}$ cells mL^{-1}. However, unlike Treatment B, the concentration of *Desulfitobacterium* spp. did not significantly change during the three cycles. In addition, the presence of *Dehalococcoides mccartyi* and 1,2-DCA dechlorination were observed at cycle 4. Rates and cell numbers of *Dehalococcoides mccartyi* continued to increase during cycle 5, with cell numbers similar

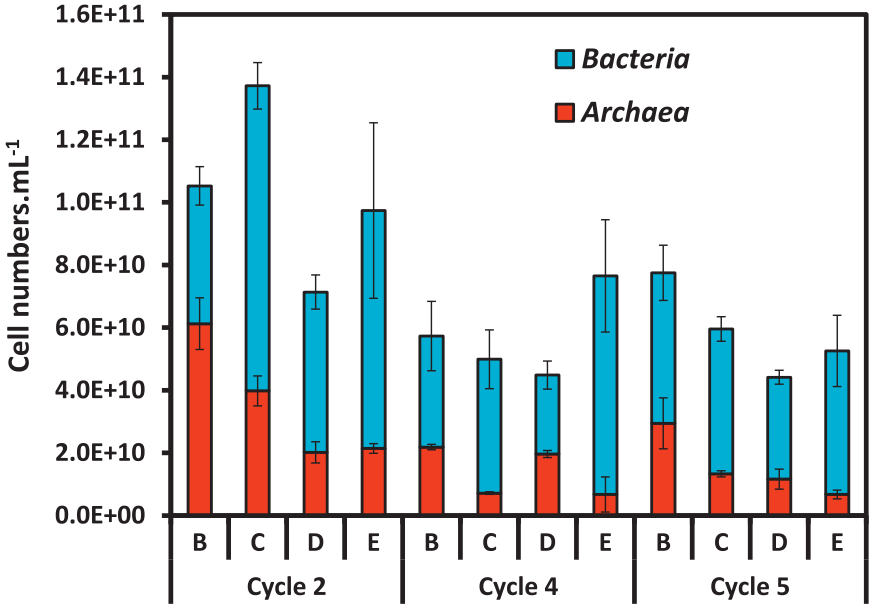

Fig. 2. Abundances of *Archaea* and *Bacteria* in microcosms not amended with magnetite (B), not amended with 1,2-DCA (C), not amended with acetate (D) and amended with all the components (E). Error bars represent the standard deviation of duplicates.

to those of *Desulfitobacterium* spp. ($1.46 \pm 0.17 \times 10^{10}$ cells mL^{-1} and $1.37 \pm 0.25 \times 10^{10}$ cells mL^{-1}, respectively) with a dechlorination rate of 2.26 μeq L^{-1} day^{-1}.

Fig. S4 shows micrographs of *Dehalococcoides mccartyi* and *Desulfitobacterium* spp. counterstained with DAPI in cycle 5 for Treatment E. The relative abundances of *Dehalococcoides mccartyi* and *Desulfitobacterium* spp. in this cycle were 33.5% and 31.7% of the total bacteria, respectively.

Treatment C showed an increasing percentage of *Desulfitobacterium* spp. during the three cycles analyzed and the relative abundance during cycle 5 (Table S1) was approximately similar to those from Treatments B and E. In comparison, the relative abundance of both *Desulfitobacterium* spp. and *Dehalococcoides mccartyi* were lower for Treatment D compared to the others.

Taken as a whole, there is a clear correlation between *Dehalococcoides mccartyi* and dechlorination, even in Treatment D in which the relative abundance was only 1.9%. In addition, the results also suggest that magnetite and 1,2-DCA played an important role in the earlier detection of *Dehalococcoides mccartyi* compared to other treatments. *Desulfitobacterium* spp. was already abundant in Treatments B through E at cycle 2 and its percentage increased over time. Since the microcosms were operated in a semi-continuous manner, this suggests that *Desulfitobacterium* spp. grew or survived on other substrates present or produced during the experimental period. Although, it is not yet known at this point what direct involvement it played in these tests but several studies have shown that *Desulfitobacterium* spp. and *Dehalococcoides mccartyi* are frequently found together (Duhamel and Edwards, 2007; Rouzeau-Szynalski et al., 2011; Villano et al., 2011).

3.4. Scanning electron microscopy and energy-dispersive X-ray spectroscopy analysis

At the end of the experiment, samples of Treatment B (without magnetite) and Treatment E (amended with all the components) were

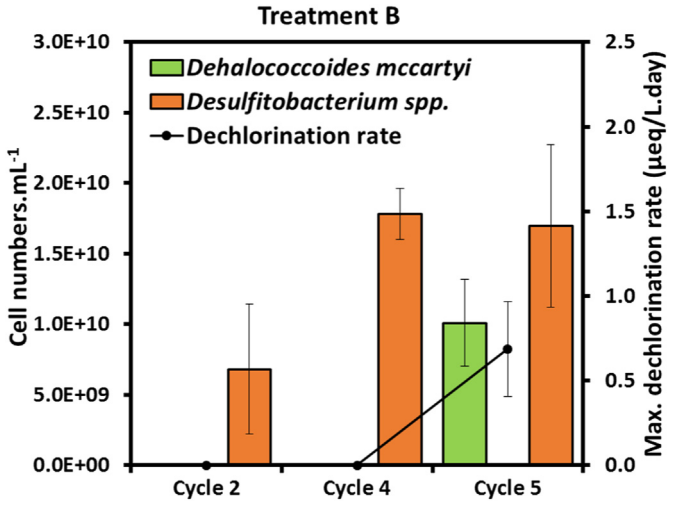

Fig. 3. Time course of *Dehalococcoides mccartyi* and *Desulfitobacterium* spp. cell densities and maximum dechlorination rates in microcosms not amended with magnetite (Treatment B). Error bars represent the standard deviation of duplicates.

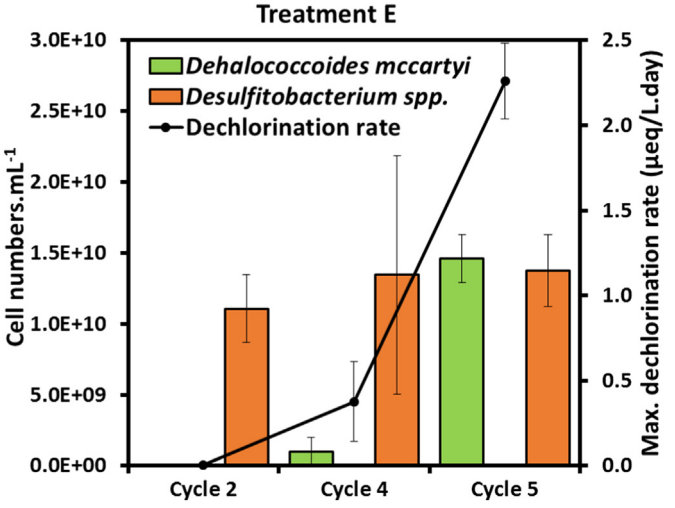

Fig. 4. Time course of *Dehalococcoides mccartyi* and *Desulfitobacterium* spp. cell densities and maximum dechlorination rates in microcosms amended with all the components (Treatment E). Error bars represent the standard deviation of duplicates.

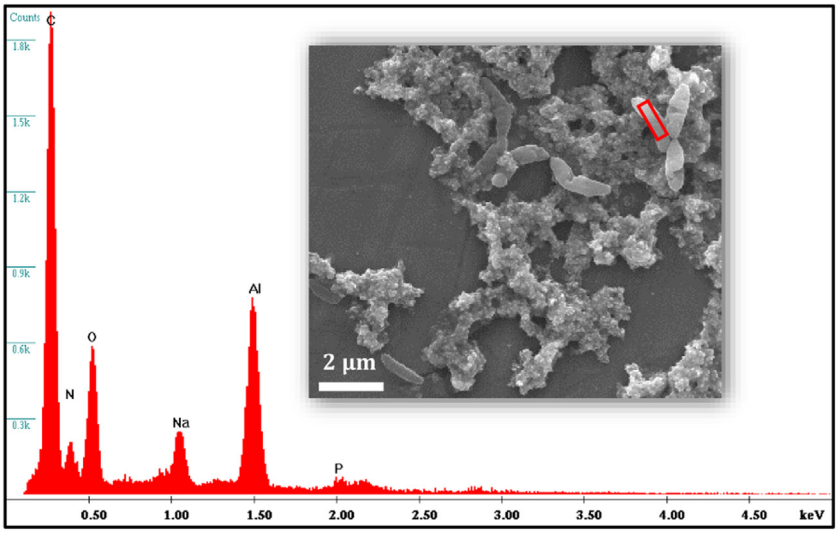

Fig. 5. SEM image of a sample from a microcosm amended with all the components (Treatment E) and the EDS spectrum corresponding to the area outlined in red.

analyzed by SEM/EDS in order to evaluate average size and morphology of magnetite particles, microorganism and as well as their relative spatial distribution. On average, magnetite particles ranged between 10 nm and 50 nm. This average size interval, although based exclusively from the visual inspection of SEM images, is consistent with that reported in literature studies employing the same magnetite synthesis protocol based on co-precipitation of Fe^{2+} and Fe^{3+} from aqueous solution under alkaline conditions (Khalil, 2015; Mascolo et al., 2013). SEM micrograph and EDS spectra of Treatment B are shown in Fig. S6. The image shows the presence of mainly rod shaped microorganisms with a length of approximately 2 µm and a composition of carbon, oxygen, nitrogen and sodium, which are characteristics of living organisms. Three different EDS analyses were performed in the same field for Treatment E but in different areas: microorganism (Fig. 5), magnetite nanoparticle (Fig. 6) and the aluminum stub (Fig. S7). Based on the spectrum shown in Fig. 5 the microorganism is mainly composed of carbon, oxygen, nitrogen and sodium, similar to the results obtained for Treatment B (Fig. S6) and confirms that the EDS was performed on biological tissue. Aluminum was also detected and can be attributed to the material onto which the sample was mounted, as later confirmed by EDS analysis performed on the background (Fig. S7). Iron precipitates were not observed and the presence of iron was not detected by EDS analysis (Fig. 5). This suggests that the microorganisms do not incorporate magnetite into their cell wall.

The EDS spectrum shown in Fig. 6 not only revealed high oxygen content, but also the presence of carbon, iron and sodium. Importantly, the background solid particles and precipitates which appear in Figs. 5, 6, and S7, and over which bacteria seemed to lay, also contained these elements, clearly indicating that they also incorporated magnetite nanoparticles. Taken as a whole, these findings suggest that bacterial cells were apparently interconnected via an electrically conductive network of nanoparticles and aggregates, thereof. Aluminum was the main element identified in a location where no visible material was present (Fig. S7) and can be attributed to the stub used to mount the sample. Also, small amounts of carbon, oxygen, and copper were detected and were probably due to extracellular exudates expelled by microorganisms. Taken as a whole, results of Figs. 5, 6, and S7 indicate that there is a close association between nanoparticles and microorganisms.

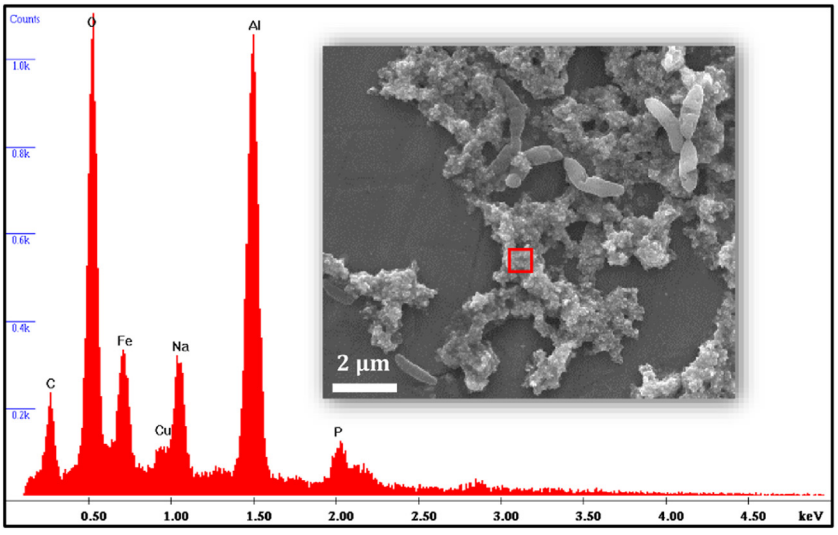

Fig. 6. SEM image of sample from microcosm amended with all the components (Treatment E) and the EDS spectrum corresponding to the area outlined in red.

When combined with the dechlorination results, this suggests that magnetite nanoparticles are serving as conduits for electron transfer between key trophic groups.

4. Conclusions

This study examined the effect of magnetite nanoparticles on 1,2-DCA dechlorination. The results demonstrated that the addition of magnetite to microcosms that contained a dechlorinating culture, 1,2-DCA and acetate had a positive influence when compared with the unamended ones. This included a 3-fold increase in dechlorination rates as well as a 20% decrease in the lag time for the onset of dechlorination. Microbial community analysis of *Archaea* showed that the concentration in the magnetite amended microcosms was lower than in unamended ones. Bacterial cell densities in magnetite-supplemented microcosms were higher than those in unamended ones. Based on the two genera of dechlorinating microorganisms analyzed, a direct correlation was established between the presence of *Dehalococcoides mccartyi* and dechlorination activity. Magnetite nanoparticles were not detected in the cell wall of the microorganisms. This suggests that this conductive mineral was not assimilated and that magnetite might only be used for interspecies extracellular electron transfer.

To the best of our knowledge, this is the first time that magnetite nanoparticles have been used to enhance 1,2-DCA dechlorination. These results may help to explain the fate of this CAH at a variety of sites, since conductive minerals are practically ubiquitous in the subsurface. Finally, future applications of these conductive nanoparticles are envisioned as a syntrophic conductive 'bio-grid' for the cleanup of contaminated groundwater.

Acknowledgements

The authors would like to thank FCT (Portuguese Foundation for Science and Technology) for the financial support of Patrícia Leitão through the PhD grant SFRH/BD/87312/2012 and to CEMUP - Centro de Materiais da Universidade do Porto for expert assistance and helpful discussions about SEM measurements.

References

Aulenta, F., Rossetti, S., Amalfitano, S., Majone, M., Tandoi, V., 2013. Conductive magnetite nanoparticles accelerate the microbial reductive dechlorination of trichloroethene by promoting interspecies electron transfer processes. ChemSusChem 6 (3), 433–436.

Aulenta, F., Fazi, S., Majone, M., Rossetti, S., 2014. Electrically conductive magnetite particles enhance the kinetics and steer the composition of anaerobic TCE-dechlorinating cultures. Process Biochem. 49 (12), 2235–2240.

Baek, G., Jung, H., Kim, J., Lee, C., 2017. A long-term study on the effect of magnetite supplementation in continuous anaerobic digestion of dairy effluent – magnetic separation and recycling of magnetite. Bioresour. Technol. 241, 830–840.

Balch, W.E., Fox, G.E., Magrum, L.J., Woese, C.R., Wolfe, R.S., 1979. Methanogens: reevaluation of a unique biological group. Microbiol. Rev. 43 (2), 260–296.

Cheng, Q., Call, D.F., 2016. Hardwiring microbes via direct interspecies electron transfer: mechanisms and applications. Environ. Sci.: Processes Impacts 18, 968–980.

Cruz Viggi, C., Rossetti, S., Fazi, S., Paiano, P., Majone, M., Aulenta, F., 2014. Magnetite particles triggering a faster and more robust syntrophic pathway of methanogenic propionate degradation. Environ. Sci. Technol. 48 (13), 7536–7543.

De Wildeman, S., Verstraete, W., 2003. The quest for microbial reductive dechlorination of C2 to C4 chloroalkanes is warranted. Appl. Microbiol. Biotechnol. 61 (2), 94–102.

De Wildeman, S., Diekert, G., Van Langenhove, H., Verstraete, W., 2003. Stereoselective microbial dehalorespiration with vicinal dichlorinated alkanes. Appl. Environ. Microbiol. 69 (9), 5643–5647.

Di Battista, A., Verdini, R., Rossetti, S., Pietrangeli, B., Majone, M., Aulenta, F., 2012. CARD-FISH analysis of a TCE-dechlorinating biocathode operated at different set potentials. New Biotechnol. 30 (1), 33–38.

Dinglasan-Panlilio, M.J., Dworatzek, S., Mabury, S., Edwards, E., 2006. Microbial oxidation of 1,2-dichloroethane under anoxic conditions with nitrate as electron acceptor in mixed and pure cultures. FEMS Microbiol. Ecol. 56 (3), 355–364.

Duhamel, M., Edwards, E.A., 2007. Growth and yields of dechlorinators, acetogens, and methanogens during reductive dechlorination of chlorinated ethenes and dihaloelimination of 1,2-dichloroethane. Environ. Sci. Technol. 41 (7), 2303–2310.

Gacitúa, M.A., González, B., Majone, M., Aulenta, F., 2014. Boosting the electrocatalytic activity of *Desulfovibrio paquesii* biocathodes with magnetite nanoparticles. Int. J. Hydrog. Energy 39 (27), 14540–14545.

Gossett, J.M., 1987. Measurement of Henry's law constants for C1 and C2 chlorinated hydrocarbons. Environ. Sci. Technol. 21 (2), 202–208.

Grostern, A., Edwards, E.A., 2009. Characterization of a *Dehalobacter* coculture that dechlorinates 1,2-dichloroethane to ethene and identification of the putative reductive dehalogenase gene. Appl. Environ. Microbiol. 75 (9), 2684–2693.

He, J., Ritalahti, K.M., Yang, K.-L., Koenigsberg, S.S., Loffler, F.E., 2003. Detoxification of vinyl chloride to ethene coupled to growth of an anaerobic bacterium. Nature 424 (6944).

Jing, Y., Wan, J., Angelidaki, I., Zhang, S., Luo, G., 2017. iTRAQ quantitative proteomic analysis reveals the pathways for methanation of propionate facilitated by magnetite. Water Res. 108, 212–221.

Kang, Y.S., Risbud, S., Rabolt, J.F., Stroeve, P., 1996. Synthesis and characterization of nanometer-size Fe_3O_4 and γ-Fe_2O_3 particles. Chem. Mater. 8 (9), 2209–2211.

Kato, S., Hashimoto, K., Watanabe, K., 2012. Microbial interspecies electron transfer via electric currents through conductive minerals. Proc. Natl. Acad. Sci. 109 (25), 10042–10046.

Khalil, M.I., 2015. Co-precipitation in aqueous solution synthesis of magnetite nanoparticles using iron(III) salts as precursors. Arab. J. Chem. 8, 279–284.

Leitão, P., Rossetti, S., Danko, A.S., Nouws, H., Aulenta, F., 2016. Enrichment of *Dehalococcoides mccartyi* spp. from a municipal activated sludge during AQDS-mediated bioelectrochemical dechlorination of 1,2-dichloroethane to ethene. Bioresour. Technol. 214, 426–431.

Liu, F., Rotaru, A.-E., Shrestha, P.M., Malvankar, N.S., Nevin, K.P., Lovley, D.R., 2012. Promoting direct interspecies electron transfer with activated carbon. Energy Environ. Sci. 5 (10), 8982–8989.

Lovley, D.R., 2017. Syntrophy goes electric: direct interspecies electron transfer. Annu. Rev. Microbiol. 71, 643–664.

Lu, X.X., Tao, S., Bosma, T., Gerritse, J., 2001. Characteristic hydrogen concentrations for various redox processes in batch study. J. Environ. Sci. Health A Tox. Hazard. Subst. Environ. Eng. 36 (9), 1725–1734.

Maes, A., Van Raemdonck, H., Smith, K., Ossieur, W., Lebbe, L., Verstraete, W., 2006. Transport and activity of *Desulfitobacterium dichloroeliminans* strain DCA1 during bioaugmentation of 1,2-DCA-contaminated groundwater. Environ. Sci. Technol. 40.

Marzorati, M., de Ferra, F., Van Raemdonck, H., Borin, S., Allifranchini, E., Carpani, G., Serbolisca, L., Verstraete, W., Boon, N., Daffonchio, D., 2007. A novel reductive dehalogenase, identified in a contaminated groundwater enrichment culture and in *Desulfitobacterium dichloroeliminans* strain DCA1, is linked to dehalogenation of 1,2-dichloroethane. Appl. Environ. Microbiol. 73 (9), 2990–2999.

Mascolo, M., Pei, Y., Ring, T., 2013. Room Temperature Co-Precipitation Synthesis of Magnetite Nanoparticles in a Large pH Window with Different Bases. Materials (Basel) 6, 5549–5567.

Maymó-Gatell, X., Chien, Y.T., Gossett, J.M., Zinder, S.H., 1997. Isolation of a bacterium that reductively dechlorinates tetrachloroethene to ethene. Science 276 (5318), 1568–1571.

Maymó-Gatell, X., Anguish, T., Zinder, S.H., 1999. Reductive dechlorination of chlorinated ethenes and 1,2-dichloroethane by "*Dehalococcoides ethenogenes*" 195. Appl. Environ. Microbiol. 65 (7), 3108–3113.

Morita, M., Malvankar, N.S., Franks, A.E., Summers, Z.M., Giloteaux, L., Rotaru, A.E., Rotaru, C., Lovley, D.R., 2011. Potential for direct interspecies electron transfer in methanogenic wastewater digester aggregates. MBio 2 (4), e00159–00111.

Rouzeau-Szynalski, K., Maillard, J., Holliger, C., 2011. Frequent concomitant presence of *Desulfitobacterium* spp. and "*Dehalococcoides*" spp. in chloroethene-dechlorinating microbial communities. Appl. Microbiol. Biotechnol. 90 (1), 361–368.

Villano, M., De Bonis, L., Rossetti, S., Aulenta, F., Majone, M., 2011. Bioelectrochemical hydrogen production with hydrogenophilic dechlorinating bacteria as electrocatalytic agents. Bioresour. Technol. 102 (3), 3193–3199.

Villano, M., Aulenta, F., Beccari, M., Majone, M., 2012. Start-up and performance of an activated sludge bioanode in microbial electrolysis cells. Chemical Engineering Transactions. Vol. 27, pp. 109–114.

Yang, Z., Guo, R., Shi, X., Wang, C., Wang, L., Dai, M., 2016. Magnetite nanoparticles enable a rapid conversion of volatile fatty acids to methane. RSC Adv. 6, 25662–25668.

Zaa, C.L.Y., McLean, J.E., Dupont, R.R., Norton, J.M., Sorensen, D.L., 2010. Dechlorinating and iron reducing bacteria distribution in a TCE-contaminated aquifer. Ground Water Monit. Rem. 30 (1), 46–57.

Zeikus, J.G., 1977. The biology of methanogenic bacteria. Bacteriol. Rev. 41 (2), 514–541.

Zhang, S., Hou, Z., Du, X.-m., Li, D.-m., Lu, X.-x., 2016. Assessment of biostimulation and bioaugmentation for removing chlorinated volatile organic compounds from groundwater at a former manufacture plant. Biodegradation 1–14.

Zhao, Z., Zhang, Y., Quan, X., Zhao, H., 2016. Evaluation on direct interspecies electron transfer in anaerobic sludge digestion of microbial electrolysis cell. Bioresour. Technol. 200, 235–244.